Predicting the Critical Gradient of ITG Turbulence in Fusion Plasmas

M.J. Pueschel[1,2,3], P.-Y. Li[4], and P.W. Terry[4]

[1]*Dutch Institute for Fundamental Energy Research, 5612 AJ Eindhoven, The Netherlands*

[2]*Eindhoven University of Technology, 5600 MB Eindhoven, The Netherlands*

[3]*Institute for Fusion Studies, University of Texas at Austin, Austin, Texas 78712, USA*

[4]*University of Wisconsin-Madison, Madison, Wisconsin 53706, USA*

Abstract

The quasilinear mixing-length approach to efficient prediction of transport in fusion devices is improved to account for the "Dimits" upshift between linear and nonlinear critical pressure gradients in zonal-flow-saturated turbulence regimes. This modification uses the frequency mismatch between modes interacting turbulently to track changes in saturation efficiency. Near criticality, energy is transfered exclusively to stable eigenmodes, rapidly increasing the efficacy of the nonlinearity. The modified quasilinear model is able to predict below-threshold turbulent ion-temperature-gradient-driven transport accurately and also yields significantly improved predictions for trapped-electron-mode transport.

Maintaining good energy confinement at high core temperatures is essential for developing fusion as an energy source. Large normalized ion temperature gradients $\omega_{T\mathrm{i}} = R_0/L_{T\mathrm{i}}$ – where R_0 is the major radius of a toroidal confinement device and $L_{T\mathrm{i}}$ the ion-temperature-gradient scale length – enable ion-temperature-gradient (ITG) instabilities to grow, develop turbulence, and produce anomalous heat fluxes. Therefore, commercial fusion reactors are predicted to operate near the marginal gradient $\omega_{T\mathrm{i,crit}}$ at which instability first arises. Significant pressure thus rests on reduced models to provide accurate predictions of heat confinement near marginality.

For ITG and other turbulence regimes that saturate via zonal flows [1], an upshift from the linear instability threshold $\omega^{\mathrm{lin}}_{T\mathrm{i,crit}}$ to the turbulence threshold $\omega^{\mathrm{NL}}_{T\mathrm{i,crit}}$, also known as the Dimits shift [2], enables experiments to attain higher core temperatures and thus improved performance.

The precise nature of what causes the Dimits shift has been elusive, in particular due to the difficulty of separating cause and effect. Thus, many attributions may be factual while not illuminating the root causes behind this phenomenon, making it difficult to design predictive models. Below $\omega^{\mathrm{NL}}_{T\mathrm{i,crit}}$, zonal flows completely dominate turbulence, with fluxes only being able to rise intermittently to low levels; non-zonal wavenumbers exhibit strongly coherent behavior. The Dimits shift is observed in a variety of scenarios [14], where it exhibits a complex dependence on collisionality, owing to non-adiabatic electron behavior, and on plasma shaping [15, 16]. In particular, it disappears at sufficiently high collision frequency.

While some theories rely on zero turbulence levels [3], fluxes are in fact small but finite and change continuously with $\omega_{T\mathrm{i}}$ throughout the Dimits regime, i.e., between the linear and nonlinear thresholds. Many approaches have focused on a sudden termination of zonal flows due to tertiary, Kelvin-Helmholtz-like [4–7] or other [8] instability: at the nonlinear threshold, zonal flows would become sufficiently strong for tertiary activity to erode zonal flows and allow turbulence to form fully. Recent work invoking tertiary instability based on zonal-flow curvature has had success in recovering turbulence onset in a fluid system [9, 10], with possible connections to one of the processes described in the present work. Alternatively, it has been proposed that stabilization of the ITG sideband, i.e., the mode at finite radial wavenumber k_x, disrupts the turbulent cascade that usually develops due to zonal-flow shearing [11]. Other theories [12, 13], based on reduced fluid models, tend to

predict critical-gradient upshifts due to zonal-flow behavior that does not match that seen in kinetics-based descriptions.

The design of fast reduced models is of great utility for understanding and predicting turbulent transport as well as for applications like real-time control. Quasilinear transport models [17–19] use a mixing-length diffusion assumption to predict turbulent electrostatic heat fluxes $Q_{\mathrm{i}}^{\mathrm{es}}$ at toroidal wavenumbers k_y based on changes in linear instability:

$$Q_{\mathrm{i}}^{\mathrm{es}} = \omega_{T\mathrm{i}} \sum_{j,k_y} C(k_y) \frac{\gamma(j,k_y) w(j,k_y)}{\langle k_\perp(k_y,j)^2 \rangle} \ , \tag{1}$$

where C is a model constant whose only dependence k_y is used to match the turbulent spectrum at one point in parameter space. Throughout this work, wavenumbers k_x and k_y are normalized to the inverse ion sound gyroradius ρ_{s}^{-1}. Furthermore, γ and w respectively denote growth rate and quasilinear weight of unstable eigenmode j at a given wavenumber, while $\langle k_\perp^2 \rangle$ is obtained by integrating the perpendicular wavenumber weighted with the square electrostatic potential and normalizing appropriately; see Ref. [20] for more details. Note that in the present analysis, only one unstable mode contributes at each k_y, although results are straightforwardly extended to multiple instabilities.

Quasilinear models are unable to recover $\omega_{T\mathrm{i,crit}}^{\mathrm{NL}}$, severely overpredicting fluxes below and only matching nonlinear trends once sufficiently far above the turbulence threshold. It is therefore essential that the source of the Dimits shift be identified and reduced models improved so they are able to predict fluxes correctly both above and within the Dimits regime.

Here, the physics of zonal-flow-based saturation are illuminated and a modified quasilinear model is deployed that accounts for the efficiency of energy transfer from the unstable ITG to stable eigenmodes, which may then return it to the background gradients. As a baseline parameter case, the ITG turbulence Cyclone Base Case in Ref. [2] is chosen, with kinetic electrons at hydrogen mass ratio and equal temperature profiles $\omega_T = \omega_{T\mathrm{i}} = \omega_{T\mathrm{e}} = 6.96$ of both species, with density gradient $\omega_n = 2.22$. The safety factor and normalized shear are $q_0 = 1.4$ and $\hat{s} = 0.796$, respectively, and local gyrokinetic [21] analysis using the GENE code [22] – for the governing equations and normalization see Ref. [23] – is performed at the flux surface with inverse aspect ratio $\epsilon_{\mathrm{t}} = 0.18$. For the normalized pressure, a near-electrostatic value of $\beta = 0.1\%$ is selected [26].

The present choice of the standard flux-tube framework allows for centering modes at

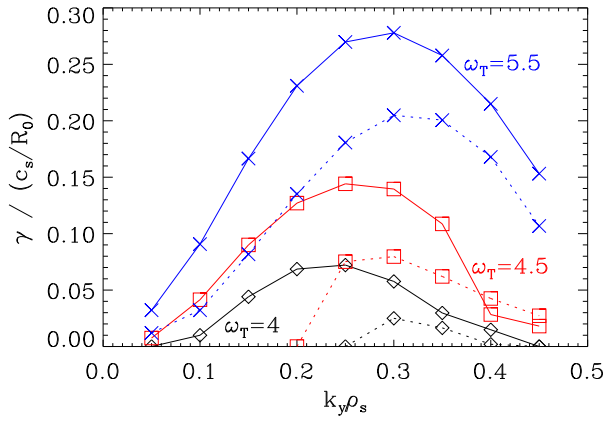

FIG. 1. Growth rates at different gradients $\omega_T = R_0/L_{T\mathrm{i}} = R_0/L_{T\mathrm{e}}$ as functions of toroidal wavenumber k_y. Solid lines correspond to modes centered at radial wavenumber $k_x = 0$, dotted lines to the sideband at $k_x = 0.1$.

$k_x \neq 0$ in ballooning representation [25], while neglecting higher-order terms in the radial expansion. Note that no conceptual changes are required to extend the present model to a radially global framework that accounts for profile effects—note, however, that non-local transients (avalanches) will require separate modeling [24]. In a situation where global profile effects become important, a potentially broad and continuous spectrum of k_x is associated with each eigenmode, making discerning of individual nonlinear interactions a more complex task. The local analysis performed here can be expected to produce quantitatively accurate results whenever local gyrokinetics is applicable – typically at values of $\rho_\mathrm{s}/a_0 \lesssim 1/100$, where a_0 denotes the minor radius – and to capture pertinent effects qualitatively in most other situations. A more detailed global analysis will be left for future work.

As evident from Fig. 1, linear growth rates γ peak in the range $0.1 < k_y < 0.5$; larger gradients lead to stronger growth, while the ITG sideband at $k_x = 0.1$ grows more slowly than the ITG streamer at $k_x = 0$. At lower k_y, the sideband becomes linearly stable for lower ω_T, whereas the streamer remains unstable.

Saturation of ITG instability occurs via zonal flows. In the following, the nonlinear interaction of streamers $k_\perp = (0, k_y)$ with the zonal flow $(0.1, 0)$ to produce sidebands $(-0.1, k_y)$ is therefore considered. One may quantify the relative importance of this particular zonal $(k_x, 0)$ thusly: At nominal parameters, in the range $k_y = 0.1 - 0.2$ where fluxes peak, modes at $k_x = 0.1 - 0.15$ show nonlinear energy transfer – which primarily arises from zonal inter-

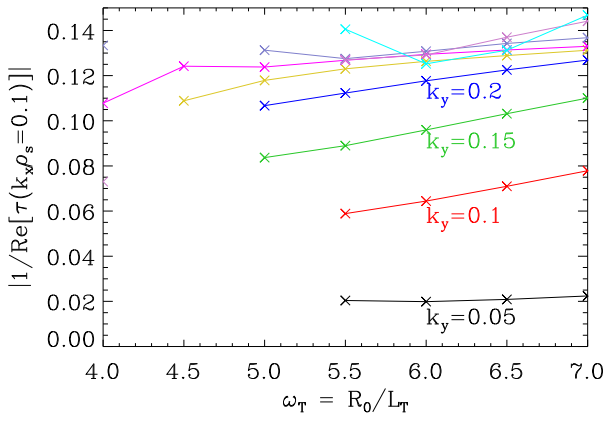

FIG. 2. The inverse of the triplet correlation time τ for unstable-to-stable energy transfer mediated by the zonal flow at $k_x = 0.1$. At $\omega_T = 7$, curves are in monotonic order of k_y with increment 0.05. Curves terminate at the gradient ω_T where the finite-k_x mode becomes stable.

actions – higher by a factor $3-5$ than those at $k_x = 0.05$. In other work [27, 28], a zonal $k_x = 0.1$ has commonly been used as a characteristic wavenumber for the zonal flow.

While the saturation mechanism of the ITG instability is commonly envisioned as shearing of turbulent eddies by the zonal flow, enhancing conservative forward energy transfer [1], the transfer is in fact strongly damped by stable-mode components of sideband fluctuations. Sidebands at low k_x also have an unstable-mode component, i.e., at low k_x they decompose into both unstable and stable modes [29]. The energy of the unstable component undergoes subsequent interaction with the $k_x = 0.1$ zonal flow, producing a cascade to the $(-0.2, k_y)$ sideband; in the flux-tube framework, the energy of the stable component is absorbed back into the equilibrium. The chain of sidebands at $(-0.2, k_y)$, $(-0.3, k_y)$, etc. carries at higher k_x a dwindlingly small fraction of the energy injected by the instability, due to depletion by the stable sideband components at each step [27]. Here, the focus lies on the first triplet of the chain, which carries the largest fraction of energy.

It is possible to quantify how efficiently a wavenumber triplet – such as streamer, sideband, and zonal flow (ZF) – interacts in the $E \times B$ quadratic nonlinearity, by evaluating the mismatch in complex frequency $\omega_c = \omega + i\gamma$ between modes as expressed by the triplet correlation time

$$\tau = \frac{1}{i\omega_c^{\mathrm{sideband}} + i\omega_c^{\mathrm{ZF}} - i(\omega_c^{\mathrm{streamer}})^*} , \tag{2}$$

which is normalized to the usual time unit R_0/c_s, with the ion sound speed c_s. As shown by a

statistical-closure calculation [30], key quantities, including the heat flux, scale as $\mathrm{Re}(\tau)^{-1}$. This property has been exploited in Refs. [31, 32] to explain and predict the nonlinear stabilization of ITG turbulence [33, 34] due to finite β. In Refs. [31, 32], linear frequencies were used as proxies for ω_c, neglecting a small nonlinear eddy-damping component. It was shown that an adequate representation of the β scaling of the heat flux can be obtained using a zero-frequency assumption $\omega_c^{\mathrm{ZF}} = 0$ for the zonal flow. Possible future improvements to this model include the use of more sophisticated zonal-flow-damping models [18].

Choosing the sideband complex frequency from quantities that can be calculated linearly is key for quasilinear modeling. However, because $\gtrsim 10^4$ linear eigenmodes exist at any given wavenumber, all of which tend to be excited [20, 35, 36], there is potentially wide latitude in choosing this frequency. Here, one can employ pseudo-eigenmode analysis, showing that nonlinear interactions favor coupling of the instability with a complex-conjugate stable mode, referred to as the ITG mirror mode, even when that mirror mode is not present in the linear eigenmode spectrum [37]. Using the mirror mode at the sideband wavenumber allows computation of the unstable-stable-zonal τ using only linear information.

Figure 2 shows the dependencies of $1/\mathrm{Re}(\tau)$ on k_y and ω_T for the present case with the $k_x = 0.1$ zonal flow; moderate stabilization with decreasing gradient is observed. More importantly, however, truncated curves indicate the disappearance of the unstable sideband ITG mode at lower gradients as the unstable k_y range contracts.

Figure 3 schematically illustrates how energy flows – mediated by the zonal mode – from the $k_x = 0$ unstable ITG streamer to subsequently higher-k_x sidebands. For each interaction, energy is split between the unstable (red diamonds) and the stable (blue squares) sideband (represented here by the mirror mode). When unstable sidebands are present at higher ω_T (top), they typically receive twice or thrice as much energy as does the stable sideband component [27]. When the sideband becomes linearly stable at lower ω_T (bottom), all energy is immediately transfered to stable eigenmodes, where it is removed from the turbulence. Thus, it becomes possible to connect continuous linear to abrupt nonlinear behavior.

Sideband stability and its variation with ω_T track the robustness of the nonlinear decorrelation of triplet interactions. These interactions are decorrelated by a bath of turbulent fluctuations at the eddy-damping rate $\Delta\omega$, an amplitude-dependent nonlinear quantity that sums over both unstable and stable modes. Because amplitudes increase with ω_T, so does $\Delta\omega$. Moreover, larger ω_T increases sideband instability, increasing the number of modes in

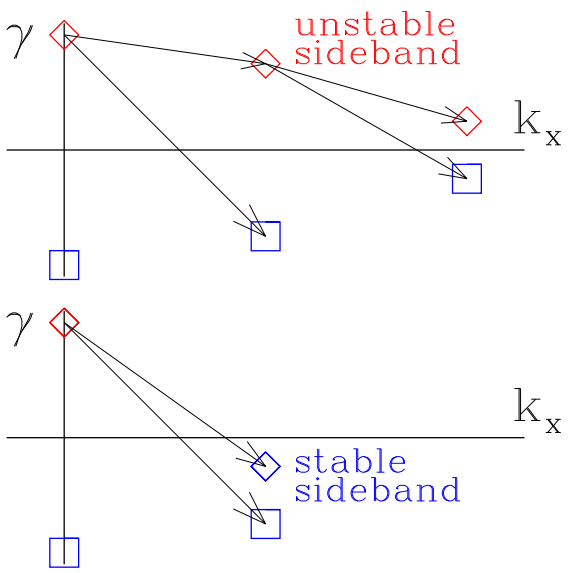

FIG. 3. Cartoon of nonlinear energy transfer (arrows) catalyzed by the zonal flow. Under normal conditions (top), energy flows from the unstable mode to both unstable (diamonds) and stable (squares) sideband modes, resulting in a non-conserving cascade to higher k_x. Near criticality, the originally-unstable sideband mode and its quasi-mirror are both stable, resulting in a higher saturation efficiency due to complete energy removal within a single nonlinear interaction.

the bath, which also increases $\Delta\omega$. This allows the use of sideband instability to track the effect of eddy damping using linear proxies for τ in calculating the heat flux from a sum of streamers.

Applying this approach to the ITG scenario at hand, a factor of $1/\mathrm{Re}(\tau)$ is included in the quasilinear flux

$$Q_{\mathrm{i}}^{\mathrm{es}} = \omega_{T\mathrm{i}} \sum_{j,k_y} C(k_y) \frac{\gamma(j,k_y) w(j,k_y)}{\langle k_\perp(k_y,j)^2 \rangle} \frac{1}{\mathrm{Re}[\tau(k_x,j)]} \ , \tag{3}$$

for individual zonal flows at a given k_x. Aside from the usual approach to drop contributions from negative growth rates, nonlinear interactions with stable sidebands are assumed to be exactly resonant, i.e.

$$\gamma(j,k_y) \to \begin{cases} \gamma(j,k_y) & \forall \ \gamma(j,k_y) > 0 \\ 0 & \forall \ \gamma(j,k_y) \leq 0 \end{cases} \ , \ \frac{1}{\mathrm{Re}[\tau(k_x,j)]} \to \begin{cases} \mathrm{Re}[\tau(k_x,j)]^{-1} & \forall \ \gamma(k_x \neq 0) > 0 \\ 0 & \forall \ \gamma(k_x \neq 0) \leq 0 \end{cases} . \tag{4}$$

This prescription, which is based entirely on linear quantities, represents nonlinear physics as follows. At low ω_T, most k_y values have a stable sideband. For these, the eddy damping

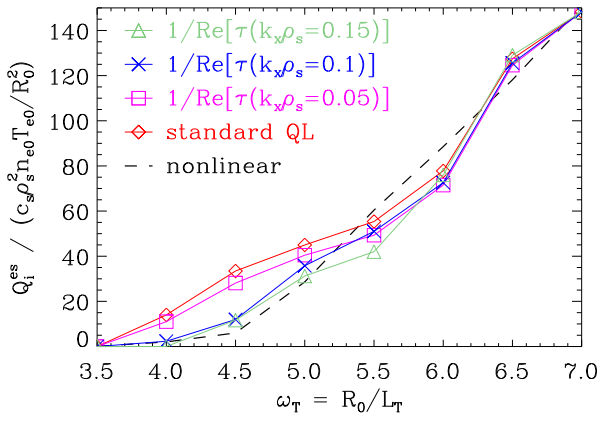

FIG. 4. Quasilinear (solid lines) and nonlinear (dashed line) fluxes as functions of temperature gradient. The standard model (red diamonds) significantly overpredicts flux at and below the nonlinear critical gradient $\omega_T \approx 4.5$, while the modified model using $\tau(k_x = 0.1)$ (blue squares) or $\tau(k_x = 0.15)$ (green triangles) reproduces the nonlinear trend. This is not the case for $\tau(k_x = 0.05)$ (pink crosses).

is very small, and the nearly resonant interaction is represented by setting $1/\mathrm{Re}(\tau) = 0$. For the few k_y values with an unstable sideband, $\Delta\omega$ is larger, and its broadening effect on resonance is represented by the linear proxy of wave dispersion, which is included in τ. At higher ω_T, there are more wavenumber values with unstable sidebands, capturing the rise of $\Delta\omega$ with ω_T. This procedure has similarities to that put forth in Ref. [11], but is rooted in an understanding of the importance of stable modes in saturation.

In Fig. 4, the dominant ion electrostatic heat fluxes (matched at $\omega_T = 7$) are shown as functions of ω_T: flux from nonlinear gyrokinetic simulations rises only once $\omega_T > 4.5$, whereas the standard quasilinear model in Eq. (1) instead predicts the nonlinear and linear thresholds to coincide, incorrectly yielding finite transport at $\omega_T \leq 4.5$. However, when accounting for unstable-ZF-sideband interactions at $k_x = 0.1$ or $k_x = 0.15$ by instead employing Eq. (3), this modified quasilinear model is able to recover the nonlinear result quantitatively at all gradients. At $\omega_T = 4$, for instance, flux predictions are lower by a factor of 6 than those based on the standard model, in large part due to the zeroing out of stable-sideband contributions to the flux. By contrast, instead basing corrections on the $k_x = 0.05$ zonal flow – which catalyzes far less nonlinear energy transfer than does the $k_x = 0.1$ zonal flow – fails to capture the upshift of the nonlinear critical gradient, and generally tracks the standard

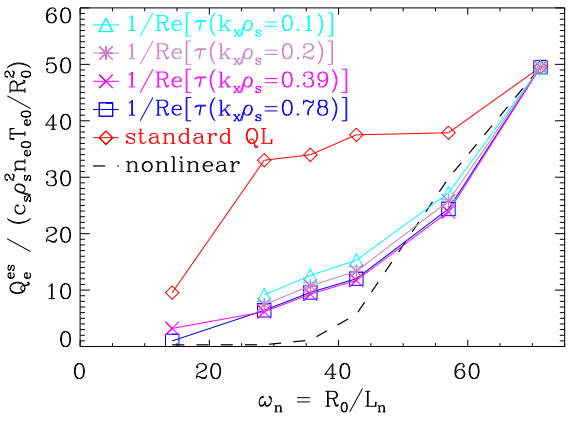

FIG. 5. Quasilinear (solid lines) and nonlinear (dashed line) fluxes as functions of density gradient for a collisionless TEM case. As for the ITG case, the standard model (red diamonds) yields poor predictions below the nonlinear threshold $\omega_n \approx 45$, whereas the τ-modified models ($k_x = 0.1$: cyan triangles; $k_x = 0.2$: purple stars; $k_x \approx 0.4$: pink crosses; $k_x \approx 0.8$: blue squares) perform significantly better, with very little sensitivity to the zonal-flow wavenumber.

quasilinear flux rather closely, as sideband stabilization is negligible at this wavenumber. Conversely, the model is insensitive to switching from $k_x = 0.1$ to 0.15. These findings are in line with nonlinear box size convergence properties.

This picture is consistent with strong coherence of fluctuations below $\omega_{T,\mathrm{crit}}$ when compared with turbulence above this point. As energy is almost instantaneously removed due to transfer to a stable sideband, no turbulent cascade develops, and strongly coherent dynamics are to be expected.

It is to be noted that a small gap between the standard and τ-corrected models is visible in Fig. 4 above $\omega_{T,\mathrm{crit}} = 4.5$, which persists for the $k_x = 0.05$ model below the nonlinear threshold. This feature is a direct result of the general decrease in inverse correlation time as per Fig. 2. As linear eigenmodes approach marginality, mode structures broaden in k_x, leading to more resonant nonlinear energy transfer within a zonal-flow triplet at a given k_x. This provides another route towards reducing fluxes near marginality and may be a more important effect than sideband stabilization in other turbulence regimes.

A separate analysis of ω_n-driven trapped-electron-mode turbulence is shown in Fig. 5, corresponding to the collisionless limit of a scenario in the Madison Symmetric Torus reversed-field pinch [38], where zonal flows are significant [39]. This strongly ω_n-driven case uses

$\omega_T = 28.8$, $\beta = 0.0141$, $q_0 = 0.103$, $\hat{s} = 6.18$, and $\epsilon_t = 0.274$. Here, all sidebands remain unstable even at density gradients below the nonlinear threshold. As the figure illustrates, using the τ-corrected model in Eq. (3) produces much-improved predictions of the heat flux over the standard model. The significant difference between the uncorrected and τ-corrected models at low density gradients stems solely from variations in τ; very little sensitivity is observed with respect to k_x, with all values from the shown range of 0.1 (the same as in Fig. 4) to 0.78 yielding essentially the same flux levels. This underscores the robustness of the model. While not shown in Fig. 5, an equivalent analysis was performed at nominal, large collisionality; there, the improved model is no longer able to predict fluxes quantitatively, as is to be expected given that nonlinear access to the stable mirror pseudo-eigenmode is no longer possible when the system becomes too dissipative.

There are other related mechanisms that can potentially contribute to the upshift of the critical gradient. One involves the nonlinear coupling coefficient for triplet interactions [30], which for the quasilinear model in Eq. (3) have been assumed to change slowly relative to τ. Explicit treatment of these coefficients requires a more involved analytical approach and will be described in a separate publication.

To summarize, an improved quasilinear transport model has been presented that, using solely linear eigenmode information as gradients are varied, is able to predict nonlinear transport behavior quantitatively both above and below the nonlinear critical gradient $\omega_{T,\mathrm{crit}}$. Two physical effects contribute to the establishment of a Dimits regime of very low transport above the linear critical gradient, by enhancing nonlinear energy transfer to stable eigenmodes: mode broadening leading to improved resonance (responsible for the upshift in the TEM case studied here) and stabilization of the linear finite-k_x sideband, thereby causing a disruption of the turbulent cascade and immediate removal of energy upon injection (responsible for the upshift for Cyclone Base Case parameters).

Implementing this approach in standard quasilinear solvers will require the ability to solve for linear eigenmodes at finite k_x. Particularly if predictions are to be possible across different turbulence regimes, a more general approach will become necessary to determine which zonal flow – if any – accounts for the bulk of nonlinear energy transfer, rather than universally setting the characteristic wavenumber to a constant $k_x = 0.1$. Ultimately, a spectral shape function in k_x – akin to what quasilinear codes might use for k_y – is envisioned, functioning as a weight function between different k_x.

While future studies will need to determine to what degree this model can be used to predict the onset of nonlinear fluxes for different turbulence regimes, the present results mark a significant advance in reduced modeling of plasma microturbulence in fusion devices, particularly for the pertinent situation of near-criticality. Furthermore, they highlight the importance of stable eigenmodes in saturation.

ACKNOWLEDGMENTS

Discussions with G.G. Whelan and J. Citrin are gratefully acknowledged. This work was supported by U.S. DOE grants DE-FG02-04ER-54742 and DE-FG02-89ER53291.

---

[1] P.H. Diamond, S.-I. Itoh, K. Itoh, and T.S. Hahm, Plasma Phys. Control. Fusion **47**, R35 (2005)

[2] A.M. Dimits *et al.*, Phys. Plasmas **7**, 969 (2000)

[3] S.-I. Itoh and K. Itoh, Nucl. Fusion **56**, 106028 (2016)

[4] B.N. Rogers, W. Dorland, and M. Kotschenreuther, Phys. Rev. Lett. **85**, 5336 (2000)

[5] R. Numata, R. Ball, R.L. Dewar, Phys. Plasmas **14**, 102312 (2007)

[6] S. Kobayashi and B.N. Rogers, Phys. Plasmas **19**, 012315 (2012)

[7] D.A. St-Onge, J. Plasma Phys. **83**, 905830504 (2017)

[8] P.G. Ivanov, A.A. Schekochihin, W. Dorland, A.R. Field, and F.I. Parra, J. Plasma Phys. **86**, 855860502 (2020)

[9] H. Zhu, Y. Zhou, and I.Y. Dodin, Phys. Rev. Lett. **124**, 055002 (2020)

[10] H. Zhu, Y. Zhou, and I.Y. Dodin, J. Plasma Phys. **86**, 905860405 (2020)

[11] M. Stransky, Phys. Plasmas **18**, 052302 (2011)

[12] K. Miki, Y. Kishimoto, N. Miyato, and J.Q. Li, Phys. Rev. Lett. **99**, 145003 (2007)

[13] G.Q. Wang, J. Ma, and J. Weiland, Phys. Scr. **90**, 065604 (2015)

[14] D.R. Mikkelsen and W. Dorland, Phys. Rev. Lett. **101**, 135003 (2008)

[15] J.E. Kinsey, R.E. Waltz, and J. Candy, Phys. Plasmas **14**, 102306 (2007)

[16] E.A. Belli, G.W. Hammett, and W. Dorland, Phys. Plasmas **15**, 092303 (2008)

[17] F. Jenko, T. Dannert, and C. Angioni, Plasma Phys. Control. Fusion **47**, B195 (2005)

[18] G.M. Staebler, J.E. Kinsey, and R.E. Waltz, Phys. Plasmas **14**, 055909 (2007)

[19] C. Bourdelle, X. Garbet, F. Imbeaux, A. Casati, N. Dubuit, R. Guirlet, and T. Parisot, Phys. Plasmas **14**, 112501 (2007)

[20] M.J. Pueschel, B.J. Faber, J. Citrin, C.C. Hegna, P.W. Terry, and D.R. Hatch, Phys. Rev. Lett. **116**, 085001 (2016)

[21] A.J. Brizard and T.S. Hahm, Rev. Mod. Phys. **79**, 421 (2007)

[22] F. Jenko and W. Dorland, Plasma Phys. Control. Fusion **43**, A141 (2001)

[23] M.J. Pueschel, F. Jenko, D. Told, and J. Büchner, Phys. Plasmas **18**, 112102 (2011)

[24] F. Rath, A.G. Peeters, R. Buchholz, S.R. Grosshauser, P. Migliano, A. Weikl, and D. Strintzi, Phys. Plasmas **23**, 052309 (2016)

[25] J. Candy, R.E. Waltz, and M.N. Rosenbluth, Phys. Plasmas **11**, 1879 (2004)

[26] W.M. Nevins, E. Wang, and J. Candy, Phys. Rev. Lett. **106**, 065003 (2011)

[27] K.D. Makwana, P.W. Terry, M.J. Pueschel, and D.R. Hatch, Phys. Rev. Lett. **112**, 095002 (2014)

[28] G.G. Whelan, Ph.D. thesis, University of Wisconsin-Madison (2019)

[29] D.R. Hatch, M.J. Pueschel, F. Jenko, W.M. Nevins, P.W. Terry, and H. Doerk, Phys. Rev. Lett. **108**, 235002 (2012)

[30] P.W. Terry, B.J. Faber, C.C. Hegna, V.V. Mirnov, M.J. Pueschel, and G.G. Whelan, Phys. Plasmas **25**, 012308 (2018)

[31] G.G. Whelan, M.J. Pueschel, and P.W. Terry, Phys. Rev. Lett. **120**, 175002 (2018)

[32] G.G. Whelan, M.J. Pueschel, P.W. Terry, J. Citrin, I.J. McKinney, W. Guttenfelder, and H. Doerk, Phys. Plasmas **26**, 082302 (2019)

[33] M.J. Pueschel, M. Kammerer, and F. Jenko, Phys. Plasmas **15**, 102310 (2008)

[34] M.J. Pueschel and F. Jenko, Phys. Plasmas **17**, 062307 (2010)

[35] D.R. Hatch, P.W. Terry, F. Jenko, F. Merz, M.J. Pueschel, W.M. Nevins, and E. Wang, Phys. Plasmas **18**, 055706 (2011)

[36] M.J. Pueschel, T. Görler, F. Jenko, D.R. Hatch, and A.J. Cianciara, Phys. Plasmas **20**, 102308 (2013)

[37] D.R. Hatch, F. Jenko, A Bañón Navarro, V. Bratanov, P.W. Terry, and M.J. Pueschel, New J. Phys. **18**, 075018 (2016)

[38] Z.R. Williams, M.J. Pueschel, P.W. Terry, and T. Hauff, Phys. Plasmas **24**, 122309 (2017)

[39] T. Nishizawa *et al.*, Phys. Rev. Lett. **122**, 105001 (2019)